On the impact of canopy model complexity on simulated carbon, water, and solar-induced chlorophyll fluorescence fluxes

Yujie Wang[1] and Christian Frankenberg[1,2]

[1]Division of Geological and Planetary Sciences, California Institute of Technology, Pasadena, California 91125, USA
[2]Jet Propulsion Laboratory, California Institute of Technology, Pasadena, California 91109, USA

Correspondence: Yujie Wang (wyujie@caltech.edu), Christian Frankenberg (cfranken@caltech.edu)

Abstract. Lack of direct carbon, water, and energy flux observations at global scales makes it difficult to calibrate land surface models (LSMs). The increasing number of remote sensing based products provide an alternative way to verify or constrain land models given its global coverage and satisfactory spatial and temporal resolutions. However, these products and LSMs often differ in their assumptions and model setups, for example, the canopy model complexity. The disagreements hamper the fusion of global scale datasets with LSMs. To evaluate how much the canopy complexity affects predicted canopy fluxes, we simulated and compared the carbon, water, and solar-induced chlorophyll fluorescence (SIF) fluxes using five different canopy complexity setups from a one-layered ~~big-leaf~~ canopy to a multi-layered canopy with leaf angular distributions. We modeled the canopy fluxes using a recently developed Land model by the Climate Modeling Alliance. Our model results suggested that (1) when using the same model inputs, model predicted carbon, water, and SIF fluxes were all higher for simpler canopy setups; (2) when accounting for vertical photosynthetic capacity heterogeneity, differences among canopy complexity levels increased compared to the scenario of a uniform canopy; (3) SIF fluxes modeled with different canopy complexity levels changed with sun-sensor geometry. Given the different modeled canopy fluxes with different canopy complexities, we recommend (1) not misusing parameters inverted with different canopy complexities or assumptions to avoid biases in model outputs, and (2) using complex canopy model with angular distribution and hyperspectral radiation transfer scheme when linking land processes to remotely sensed spectra.

1 Introduction

Land surface models (LSMs) simulate the carbon, water, and energy fluxes at the land–atmosphere interface at regional and global scales, and are key component for Earth system models (ESMs). The ability of LSMs to accurately model the carbon, water, and energy fluxes within vegetation canopy largely determines the predictive skills of the ESMs. Modeling canopy carbon, water, and energy fluxes dates back to the early 20th century, and various canopy models with different complexities from single layer to multiple layers (see Bonan et al. (2021) for an overview). To date, the most widely used canopy ~~model in various land surface models (LSMs) is the commonly known big-leaf model , which considers the canopy as a big leaf with sunlit and shaded fractions (Campbell and Norman, 1998) .~~ models in LSM community are the "big leaf model family".

The biggest advantage of the ~~big-leaf model~~ big leaf model family is computational efficiency given the simple mathematical formulation. The potential disadvantages of the ~~big-leaf model~~ big leaf model family are also obvious, e.g., the model is too simplified and thus not able to resolve vertically varying profiles and microclimates in the canopy, such as air temperature, humidity, and wind speed (Bonan et al., 2021). Thus, there is an increasing demand for LSMs to move from simple one-layered ~~big-leaf~~ canopy to a multi-layered one.

One of the most important functionality of canopy models is to predict carbon, water, and energy fluxes globally in the future to determine whether the land will remain a carbon sink. Though canopy models with different complexity levels have been extended to global scale in different LSMs, researchers are facing a key problem: a lack of direct global scale carbon, water, and energy flux observations. The lack of data makes it difficult to calibrate the LSMs at global scales, particularly those using more complex canopy setups given the more parameters required. As a result, though it is shown that a multi-layered canopy model better resolves ~~the~~ energy fluxes in the canopy (Bonan et al., 2021), ~~it is not yet able to determine whether~~ limited is known about will the multi-layered canopy ~~model will outperform and succeed the big-leaf model at global scales in existing LSMs,~~ models show improved predictive skills (particularly in terms of carbon and water fluxes) compared to the big leaf models which are widely used in existing LSMs.

To better constrain LSMs with data, people realized the promise of remote sensing data given its global coverage and satisfactory spatial and temporal resolutions. Regarding carbon, research has shown that solar-induced chlorophyll fluorescence (SIF) and near infrared reflection of vegetation (NIRv) are correlated with plant primary productivity (GPP; Frankenberg et al.,

2011; Zhang et al., 2016; Sun et al., 2018; Badgley et al., 2019). Regarding water, researchers also found SIF being useful to

60 invert transpiration rate by prescribing stomatal responses to the environment (e.g., Shan et al., 2021), and vegetation optical depth in sensing above ground biomass and canopy water stress (Momen et al., 2017; Zhang et al., 2019). Regarding energy, various models and algorithms have been used to detect surface energy balance using optical light and microwave (e.g., Roerink et al., 2000; Norman et al., 2003). Further, methods and applications have been developed to invert plant traits from remote sensing data, such as leaf area index (e.g., Colombo et al., 2003; Deng et al., 2006) and chlorophyll content (Croft et al., 2020).

65 Despite the increasing number of inverted fluxes and plant traits datasets, limited research has tested the capability of these data in improving LSM predictions. Among the various reasons that hamper the fusion of large scale datasets into LSMs, incompatibility between model and data assumptions seems to be the major reason. For example, the disagreement in canopy complexity may introduce errors into modeling if one uses the data inverted from a canopy complexity level (e.g., ~~big-leaf~~ one-layered canopy) in a model with a different canopy complexity level (e.g., multi-layered canopy). Further, the flux and

70 trait maps inverted from remote sensing data often use simplified plant physiological representations, which are, however, key processes in land modeling. For example, studies that derive GPP from SIF or NIRv often assume linear correlation between them, whereas vegetation models must account for light saturation (Zhang et al., 2016).

Ideally, LSMs can be constrained using raw reflection and fluorescence spectra. This, nevertheless, requires the LSMs moving from broadband canopy radiation to a hyperspectral representation, and from sunlit and shaded fractions to leaf angular

75 distributions (such as the land model developed by Climate Modeling Alliance, CliMA Land; Wang et al., 2021b). This way, the LSM can be directly coupled to remotely sensed canopy spectra (e.g., Shiklomanov et al., 2021) rather than to reprocessed datasets using often incompatible assumptions. The increasing canopy complexity, however, comes with high costs: (a) much more computational resources required by increasing amount of leaves (e.g., CliMA Land canopy has a default of 6500 leaves per tree in the canopy whereas ~~big-leaf~~ two-leaf canopy has 2 "leaves"), (b) more complicated canopy radiation and fraction

80 (e.g., CliMA Land model calculates the radiation and fraction based on leaf angular distribution for a default of 6500 leaves), and (c) most importantly, increasing difficulty for research communities to understand or use the model.

To resolve the problems of a complicated canopy, we examined how much carbon, water, and SIF fluxes may differ when using different canopy complexity representations in CliMA Land model, spanning from one-layered ~~big-leaf~~ canopy to multi-layered canopy with hyperspectral radiation and leaf angular distributions (Figure 1). With the model simulations, we were able

85 to answer (1) how does canopy complexity impact modeled canopy fluxes, and (2) could data inverted using different canopy complexity levels be compatible. Regarding the ease of understanding and using a LSM with various canopy complexities, we presented and suggested the highly modularized CliMA Land model which can be easily set up to simulate canopy fluxes using different canopy complexity levels.

2 Materials and Methods

90 We used the CliMA Land model (v0.1) to evaluate how canopy model complexity impacts the simulated carbon, water, and SIF fluxes. The CliMA Land model mechanistically addresses soil-plant-air continuum processes, and is able to simulate canopy
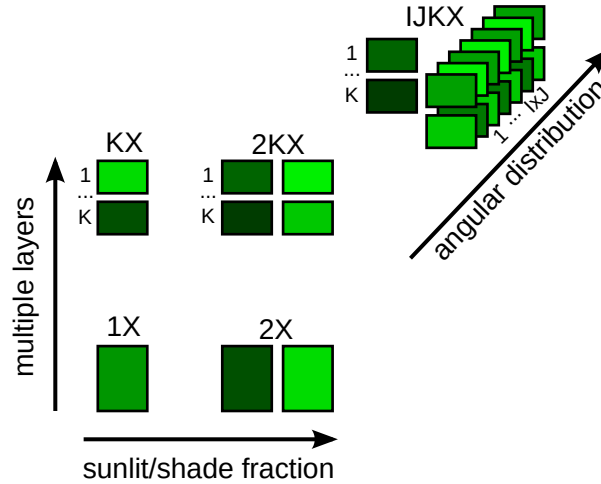
Figure 1. Canopy complexity levels. "1X": single layer canopy without sunlit or shaded fractions. "2X": single layer canopy with sunlit and shaded fractions. "KX": multiple layer canopy without sunlit or shaded fractions. "2KX": multiple layer canopy with sunlit and shaded fractions per layer. "IJKX": multiple layer canopy with sunlit and shade fractions per layer, and the sunlit fraction is further partitioned based on leaf inclination and azimuth angular distributions.

carbon and water fluxes as well as SIF simultaneously (Wang et al., 2021b). Code and documentation of the CliMA Land model are freely and publicly available at https://github.com/CliMA/Land.

2.1 Canopy complexity levels

95 Leaf physiological responses to light are highly non-linear, such as stomatal conductance to water vapor (g_{sw}) and net photosynthetic rate (A_{net}). Typically, when absorbed photosynthetically active radiation (APAR) is low, g_{sw} and A_{net} increase with higher APAR (Figure 2a); when APAR is high, g_{sw} and A_{net} saturate. If one has a leaf with a low APAR and a leaf with a high APAR (e.g., closed circles on the solid curves of Figure 2a), the mean behavior of the two leaves ought to be the average g_{sw} and A_{net} values (closed circles on the colored dashed lines of Figure 2a). However, if one uses the mean APAR of the two

100 leaves, and calculates g_{sw} and A_{net} based on the mean APAR, g_{sw} and A_{net} would be overestimated (open circles on the colored solid curves of Figure 2a). Note that averaging APAR values that are beyond the turning point, say 350 μmol m^{-2} s^{-1}, may not result in any bias in modeled g_{sw} and A_{net} (such as for sunlit and shaded leaves in the top canopy layer); however, averaging APAR for leaves with high APAR and low APAR, say 300 and 50 μmol m^{-2} s^{-1} would result in overestimated g_{sw} and A_{net} (such as for shaded leaves in upper and lower canopy as typically done in the two-leaf radiation scheme). Thus, overly simpli-

105 fied canopy model may overestimate canopy level carbon and water fluxes because of the inappropriately averaged APAR, as $f(\overline{x}) \neq \overline{f(x)}$ when averaging nonlinear functions ($A_{net}(\overline{APAR}) > \overline{A_{net}(APAR)}$ in leaf photosynthesis).

To evaluate how much canopy model complexity matters, we modeled the canopy using five different levels of complexity, and they are denoted as "1X", "2X", "KX", "2KX", and "IJKX" (Figure 1). "1X" represents the scenario in which the
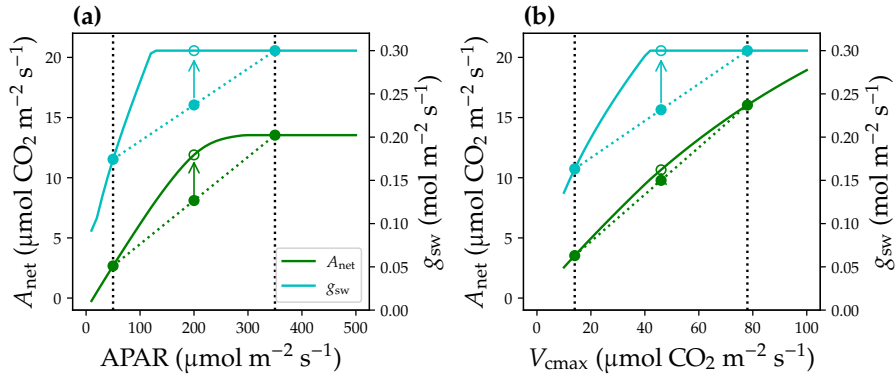
Figure 2. Non-linear leaf responses to the environmental and physiological parameters. **(a)** Stomatal conductance to water vapor (g_{sw}; cyan solid curve) and net photosynthetic rate (A_{net}) responses to absorbed photosynthetically active radiation (APAR). The black dotted vertical lines indicate two leaves at low and high light conditions. Mean behavior of the two leaves ought to be the closed circles on the colored dotted lines. However, use mean APAR for the leaves would result in overestimated g_{sw} and A_{net} (open circles). **(b)** Non-linear g_{sw} and A_{net} responses to leaf photosynthetic capacity, represented by maximum carboxylation rate (V_{cmax}). Environmental and leaf physiological settings for the simulations are: air and leaf temperatures at 298.15 K, atmospheric vapor pressure at 1500 Pa (relative humidity at 0.47), atmospheric CO_2 partial pressure at 40 Pa, atmospheric pressure at 101325 Pa, V_{cmax} (for panel a) at 60 μmol m^{-2} s^{-1}, and maximal stomatal conductance at 0.3 mol m^{-2} s^{-1}.

canopy is treated as a single ~~big~~ average leaf without sunlit or shaded fractions, and leaf radiation is averaged for the en-

110 tire canopy. "2X" complicates "1X" by partitioning the ~~big~~ average leaf to sunlit and shaded fractions. "KX" enhances the "1X" by partitioning the canopy to multiple layers (but no sunlit or shaded fractions per layer). "2KX" partitions each canopy layer of "KX" to sunlit and shaded fractions. "IJKX" further modifies "2KX" by accounting for leaf inclination and az-imuth angle distributions per layer (Figure 1). ~~We note here that "2X" resembles the commonly used big-leaf canopy in most~~ ~~LSMs such as the Community Land Model (CLM), "KX" resembles the multi-layered Organising Carbon and Hydrology In~~

115 ~~Dynamic Ecosystems LSM (ORCHIDEE; Chen et al., 2016; Ryder et al., 2016) ; "2KX" resembles the multi-layered version~~ ~~CLM (CLM-ml; Bonan et al., 2018, 2021) and "lite on" option of Soil-Canopy Observation of Photosynthesis and Energy~~ ~~fluxes (SCOPE v2.0; Yang et al., 2021) ; and "IJKX" resembles the "lite off" option of SCOPE (v2.0; Yang et al., 2021) .~~ See Table 1 for the canopy model complexity adopted by other vegetation models (see https://yujie-w.github.io/PAGES/dev/ methods/#Vegetation-canopy-model-complexity for a growing list).

120 For "IJKX", we simulated the canopy radiative transfer using the CliMA Land adapted SCOPE model (SCOPE v1.7; Yang et al., 2017). The adaptations included that carotenoid absorption was accounted as APAR (Wang et al., 2021b) and that canopy clumping was addressed using a clumping index (Braghiere et al., 2021). At layer i, the shaded leaf fraction (relative to total leaf area in the canopy) is $p_{sh,i}$, and the sunlit leaf fraction (relative to total leaf area in the canopy) is $p_{sl,i}$(incl, azi) ("incl" is the inclination angle, and "azi" is the azimuth angle). The fraction of sunlit leaves relative to total canopy leaf area in a given

Table 1. A list of vegetation models that corresponds to our tested canopy complexity schemes.

Model	Version	Reference	Complexity
CLM	4	Bonan et al. (2011)	2X
	5	Lawrence et al. (2019)	2X
	ml	Bonan et al. (2018)	2KX
ISBA	A-gs	Carrer et al. (2013)	2KX
	MEB	Boone et al. (2017)	2KX
JULES	can_rad_mod 1	Jogireddy et al. (2006)	one-big-leaf
	can_rad_mod 4	Clark et al. (2011)	IJKX
	can_rad_mod 5	Clark et al. (2011)	2KX
ORCHIDEE	CAN v1	Ryder et al. (2016)	KX
SCOPE	1	Van der Tol et al. (2009)	IJKX
	2, lite off	Yang et al. (2021)	IJKX
	2, lite on	Yang et al. (2021)	2KX

canopy layer is computed as

$$\sum_{\text{incl,azi}} p_{\text{sl,i}}(\text{incl,azi}) = \frac{\text{LAI(i+1)} - \text{LAI(i)}}{\text{LAI}} \cdot \int_{\text{LAI(i)}}^{\text{LAI(i+1)}} \exp(-k\Omega x) \cdot \mathrm{d}x, \tag{1}$$

where LAI is total leaf area index, LAI(i) is the leaf area index above the ith canopy layer, LAI(i) is the leaf area index in and above the ith canopy layer, k is the distinction coefficient as a function of leaf inclination angle distribution, and Ω is the clumping index. Then $p_{\text{sl,i}}(\text{incl,azi})$ is computed using

$$p_{\text{sl,i}}(\text{incl,azi}) = \sum_{\text{incl,azi}} p_{\text{sl,i}}(\text{incl,azi}) \cdot \frac{1}{I} \cdot \frac{1}{J}, \tag{2}$$

where I is the number of inclination angles and J is the number of azimuth angle. The fraction of shaded leaves relative to total canopy leaf area in a given canopy layer is computed as

$$p_{\text{sh,i}} = \frac{\text{LAI(i+1)} - \text{LAI(i)}}{\text{LAI}} \cdot \left[1 - \int_{\text{LAI(i)}}^{\text{LAI(i+1)}} \exp(-k\Omega x) \cdot \mathrm{d}x \right]. \tag{3}$$

Corresponding APAR for the shaded and sunlit leaves are APAR_{sh} and $\text{APAR}_{\text{sl,i}}(\text{incl, azi})$, respectively. We used a default $I = 9$ inclination angles, $J = 36$ azimuth angles, $K = 20$ vertical layers for "IJKX" ($K = 20$ for for "2KX" and "KX" as well).

"2KX" fraction and APAR were derived from the "IJKX" by weighing the APAR for sunlit leaves per canopy layer:

$$^{2KX}p_{sl,i} = \sum_{incl,azi} p_{sl,i}(incl,azi);$$

$$^{2KX}p_{sh,i} = p_{sh,i};$$

$$^{2KX}APAR_{sl,i} = \frac{\sum_{incl,azi}\left[APAR_{sl,i}(incl,azi) \cdot p_{sl,i}(incl,azi)\right]}{\sum_{incl,azi}\left[p_{sl,i}(incl,azi)\right]};$$

$$^{2KX}APAR_{sh,i} = APAR_{sh,i}. \tag{4}$$

"KX" fraction and APAR were derived from the "2KX" by weighing the APAR for all sunlit and shaded leaves per canopy layer:

$$^{KX}p_i = {}^{2KX}p_{sl,i} + {}^{2KX}p_{sh,i};$$

$$^{KX}APAR_i = \frac{{}^{2KX}APAR_{sl,i} \cdot {}^{2KX}p_{sl,i} + {}^{2KX}APAR_{sh,i} \cdot {}^{2KX}p_{sh,i}}{{}^{KX}p_i}. \tag{5}$$

"2X" fraction and APAR were derived from the "2KX" by weighing the APAR for sunlit and shaded leaves for all canopy layers, respectively:

$$^{2X}p_{sl} = \sum_i p_{sl,i};$$

$$^{2X}p_{sh} = \sum_i p_{sh,i};$$

$$^{2X}APAR_{sl} = \frac{\sum_i\left({}^{2KX}APAR_{sl,i} \cdot {}^{2KX}p_{sl,i}\right)}{\sum_i\left({}^{2KX}p_{sl,i}\right)};$$

$$^{2X}APAR_{sh} = \frac{\sum_i\left({}^{2KX}APAR_{sh,i} \cdot {}^{2KX}p_{sh,i}\right)}{\sum_i\left({}^{2KX}p_{sh,i}\right)}. \tag{6}$$

"1X" APAR was derived from the "KX" by weighing the APAR for all layers:

$$^{1X}APAR = \sum_i\left({}^{KX}APAR_i \cdot {}^{KX}p_i\right). \tag{7}$$

We emphasize here that to derive canopy fluorescence spectrum and its sun-sensor geometry, we need to simulate the canopy radiative transfer using hyperspectral reflectance, transmittance, and fluorescence. Due to the high spectral resolution and multiple layers required, radiative transfer and canopy fractions in complex models such as SCOPE are computed numerically. In comparison, radiative transfer and sunlit/shaded fractions are computed analytically in the two-leaf radiation scheme as the model is single layered and uses broadband reflectance and transmittance (Campbell and Norman, 1998; Bonan et al., 2021). Yet, the two-leaf radiation scheme that use broadband radiative transfer are not adequate for accurate fluorescence modeling. Crucially, the difference in the analytic and numerical solutions could result in biases in the simulated APAR and fraction. To avoid such bias, we computed the APAR and sunlit/shaded fractions for the simpler canopy setups numerically using the algorithm in "IJKX". See Figure 3 for the APAR profiles for "2KX", "KX", "2X", and "1X" derived from "IJKX". Also, we

155 note here that leaf biochemical parameters and APAR were not integrated within a canopy layer or sunlit/shaded fractions; instead, we used average APAR and leaf traits in our simulations. Thus, our "1X" model is a one-leaf model rather than a one-big-leaf model, and our "2X" model resembles the two-leaf model rather than two-big-leaf model.
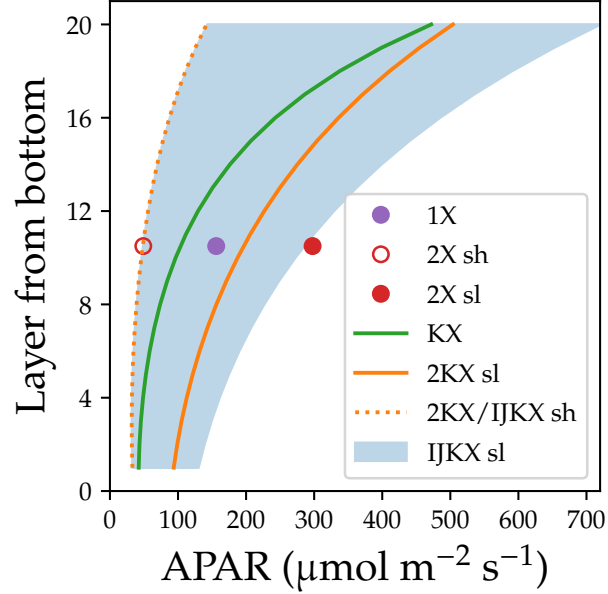
Figure 3. Comparison of mean absorbed photosynthetically active radiation (APAR) profiles for four different canopy complexity levels. "1X": single layer canopy without sunlit or shaded fractions. "2X": single layer canopy with sunlit and shaded fractions. "KX": multiple layer canopy without sunlit or shaded fractions. "2KX": multiple layer canopy with sunlit and shaded fractions per layer. "IJKX": multiple layer canopy with sunlit and shade fractions per layer, and the sunlit fraction is further partitioned based on leaf inclination and azimuth angular distributions. The "sl" and "sh" stand for sunlit and shaded leaves, respectively.

2.2 Vertical canopy profile

Leaf traits in the canopy are not uniform among the canopy layers. Typically, leaf photosynthetic capacity (usually represented
160 by maximum carboxylation rate at 25 °C, V_{cmax}) is higher in upper canopy because of the better light environment. Further, leaf physiological responses to V_{cmax} are also highly non-linear, and using average V_{cmax} may also result in overestimated g_{sw} and A_{net}, and thus carbon and water fluxes (e.g., shift from solid circles to open circles in Figure 2b).

To examine how much the vertical V_{cmax} profile impacts modeled canopy flux simulations, we ran the model simulation in two scenarios, one using uniform V_{cmax} in the canopy and one using decreasing V_{cmax} towards the lower canopy. For the latter
165 scenario, V_{cmax} at layer i was tuned using an exponential function following De Pury and Farquhar (1997) and Chen et al. (2012):

$$V_{cmax,i} = V_{cmax,top} \cdot \exp\left[-0.15 \cdot LAI(i)\right], \tag{8}$$

where $V_{\text{cmax,top}}$ is the V_{cmax} at the top of the canopy, and 0.15 is the shape factor that describes the decreasing V_{cmax} with canopy depth, and LAI(i) is the leaf area index above the ith canopy layer. Note that as leaves are experiencing dynamically changing light environment throughout the day, it is unrealistic to assume the sunlit and shaded leaves have different traits; thus, we only accounted for the vertical heterogeneity but neglected the horizontal heterogeneity in each canopy layer, namely using the same characteristics for leaves within the same canopy layer.

V_{cmax} profile was applied to "IJKX", "2KX" and "KX" directly, whereas weighed mean $V_{\text{cmax}} = \sum_i V_{\text{cmax,i}} \cdot^{\text{KX}} p_i$ was used in "1X". The V_{cmax} profile or value stayed constant in these four scenarios throughout the simulation as sunlit/shaded fractions did not impact them. We note here that mean V_{cmax} changed with sunlit/shaded fractions in "2X" (Chen et al., 2012), and particular averages of V_{cmax} for sunlit and shaded fractions ($^{2X}V_{\text{cmax,sl}}$ and $^{2X}V_{\text{cmax,sh}}$, respectively) need to be updated with sunlit and shaded fractions:

$$^{2X}V_{\text{cmax,sl}} = \frac{\sum_i \left({}^{2KX}V_{\text{cmax,i}} \cdot {}^{2KX}p_{\text{sl,i}} \right)}{\sum_i \left({}^{2KX}p_{\text{sl,i}} \right)};$$
$$^{2X}V_{\text{cmax,sh}} = \frac{\sum_i \left({}^{2KX}V_{\text{cmax,i}} \cdot {}^{2KX}p_{\text{sh,i}} \right)}{\sum_i \left({}^{2KX}p_{\text{sh,i}} \right)}. \tag{9}$$

Note that we tuned maximum electron transport rate and leaf respiration rate in the same manner as V_{cmax}.

2.3 Canopy flux simulations

We simulated the canopy carbon and water fluxes using a stomatal optimization model developed in Wang et al. (2020) given the good model performance and scalability (Wang et al., 2021a). The stomatal optimization model posits that stomatal opening is optimized when the difference between carbon gain and risk is maximum:

$$\max \underbrace{A_{\text{net}}}_{\text{gain}} - \underbrace{A_{\text{net}} \cdot \frac{E}{E_{\text{crit}}}}_{\text{risk}}, \tag{10}$$

where E is the leaf transpiration rate, and E_{crit} is the critical transpiration rate of the leaf beyond which leaf hydraulic conductance drops below 0.1% of the maximum (see Sperry et al. (2016) and Wang et al. (2021b) for more details of E_{crit}).

At each canopy complexity level, for a given environmental condition set, we were able to obtain the steady state stomatal conductance for each APAR, from which we computed steady state A_{net} using the classic C3 photosynthesis model (Farquhar et al., 1980) and E as well as leaf fluorescence quantum yield (ϕ_{F}) using the model developed in van der Tol et al. (2014). Stand level carbon flux, namely net ecosystem exchange (NEE; normalized per ground area) was computed using

$$\text{NEE} = \text{LAI} \cdot \sum \left(A_{\text{net}} \cdot p \right) - R_{\text{remain}};$$

$$\text{NEE} = \text{LAI} \cdot \sum A_{\text{net}} \cdot p - R_{\text{remain}}.$$

$$^{\text{IJKX}}\text{NEE} = \text{LAI} \cdot \sum_{i,\text{incl,azi}} [A_{\text{net}}(\text{APAR}_{\text{sl,i}}(\text{incl,azi})) \cdot p_{\text{sl,i}}(\text{incl,azi})] + \text{LAI} \cdot \sum_i [A_{\text{net}}(\text{APAR}_{\text{sh,i}}) \cdot p_{\text{sh,i}}] - R_{\text{remain}};$$

$$^{\text{2KX}}\text{NEE} = \text{LAI} \cdot \sum_i \left[A_{\text{net}} \left(^{\text{2KX}}\text{APAR}_{\text{sl,i}}\right) \cdot^{\text{2KX}} p_{\text{sl,i}} + A_{\text{net}} \left(^{\text{2KX}}\text{APAR}_{\text{sh,i}}\right) \cdot^{\text{2KX}} p_{\text{sh,i}} \right] - R_{\text{remain}};$$

$$^{\text{KX}}\text{NEE} = \text{LAI} \cdot \sum_i \left[A_{\text{net}} \left(^{\text{KX}}\text{APAR}\right) \cdot^{\text{KX}} p_i \right] - R_{\text{remain}};$$

$$^{\text{2X}}\text{NEE} = \text{LAI} \cdot A_{\text{net}} \left(^{\text{2X}}\text{APAR}_{\text{sl}}\right) \cdot^{\text{2X}} p_{\text{sl}} + \text{LAI} \cdot A_{\text{net}} \left(^{\text{2X}}\text{APAR}_{\text{sh}}\right) \cdot^{\text{2X}} p_{\text{sh}} - R_{\text{remain}};$$

$$^{\text{1X}}\text{NEE} = \text{LAI} \cdot A_{\text{net}} \left(^{\text{1X}}\text{APAR}\right) - R_{\text{remain}}. \tag{11}$$

where LAI is leaf area index, and R_{remain} is the ecosystem respiration rate per ground area excluding the leaves. The transpiration rate from the canopy is computed and used as a proxy for estimating the difference in model ecosystem evapotranspiration (ET; normalized per ground area) using $\text{ET} \approx \text{LAI} \cdot \sum (E \cdot p)$

$$\text{ET} = \text{LAI} \cdot \sum E \cdot p.$$

$$^{\text{IJKX}}\text{ET} \approx \text{LAI} \cdot \sum_{i,\text{incl,azi}} [E(\text{APAR}_{\text{sl,i}}(\text{incl,azi})) \cdot p_{\text{sl,i}}(\text{incl,azi})] + \text{LAI} \cdot \sum_i [E(\text{APAR}_{\text{sh,i}}) \cdot p_{\text{sh,i}}];$$

$$^{\text{2KX}}\text{ET} \approx \text{LAI} \cdot \sum_i \left[E \left(^{\text{2KX}}\text{APAR}_{\text{sl,i}}\right) \cdot^{\text{2KX}} p_{\text{sl,i}} + E \left(^{\text{2KX}}\text{APAR}_{\text{sh,i}}\right) \cdot^{\text{2KX}} p_{\text{sh,i}} \right];$$

$$^{\text{KX}}\text{ET} \approx \text{LAI} \cdot \sum_i \left[E \left(^{\text{KX}}\text{APAR}\right) \cdot^{\text{KX}} p_i \right];$$

$$^{\text{2X}}\text{ET} \approx \text{LAI} \cdot E \left(^{\text{2X}}\text{APAR}_{\text{sl}}\right) \cdot^{\text{2X}} p_{\text{sl}} + \text{LAI} \cdot E \left(^{\text{2X}}\text{APAR}_{\text{sh}}\right) \cdot^{\text{2X}} p_{\text{sh}};$$

$$^{\text{1X}}\text{ET} \approx \text{LAI} \cdot E \left(^{\text{1X}}\text{APAR}\right). \tag{12}$$

We remind here that soil evaporation is a function of soil water content, soil surface temperature, and atmospheric vapor pressure deficit, and that soil evaporation should be the same for all tested canopy complexity models; so does for evaporation from intercepted water on plant surface. Therefore, the modeled ET difference is 100% caused by canopy transpiration, and using transpiration would not result in any biases in the relative difference of modeled ET.

For "IJKX", we used ϕ_F computed for each sunlit and shaded leaf at each layer to compute canopy level SIF spectrum. For "2KX", we plugged the ϕ_F calculated for sunlit fraction into all the sunlit leaves of the corresponding layer of "IJKX", and the shaded ϕ_F to the shaded leaf of the corresponding layer of "IJKX". Then we re-simulate re-simulated the SIF spectrum at "IJKX" and used it as that of "2KX". For "KX", we plugged the ϕ_F calculated for the whole layer into all the leaves of

corresponding layer of "IJKX", and recalculated the SIF spectrum. For the "2X", we plugged the ϕ_F of sunlit fraction to all the sunlit leaves in "IJKX" and shaded ϕ_F to all the shaded leaves in "IJKX", and recalculated the SIF spectrum. For "1X", we plugged the ϕ_F into all the leaves in "IJKX", and recalculate the SIF spectrum. We compared SIF at 740 nm (SIF_{740}) among different complexity levels.

210   Despite the importance of vertical microclimate heterogeneity in modeled canopy energy fluxes (e.g., Bonan et al., 2021), we held environmental conditions constant among vertical canopy layers for all tested canopy complexities. Doing this allowed us to tease apart the impact of APAR distribution in the canopy (due to canopy complexity) on simulated carbon, water, and SIF fluxes.

2.4   Sensitivity analysis

215   We ran a sensitivity analysis to environmental cues for all five complexity levels to examine how ~~they much~~ much they differ in predicted carbon, water, and SIF fluxes. The tested cues included solar radiation, atmospheric vapor pressure deficit (VPD), temperature, soil water potential (Ψ_{soil}), and atmospheric CO_2 partial pressure (P_{CO2}). When we altered temperature, we changed the air and leaf temperature at the same time and held air ~~humidity~~ relative humidity (RH) constant at 0.47 (~~a~~ fraction; unitless). Saturated water vapor pressure ~~of 1500 Pa at 25 °C).~~ was computed using the Clapeyron–Clausius equation

$$P_{sat} = P_{triple} \cdot \left(\frac{T}{T_{triple}} \right)^{\frac{\Delta c_p}{R_v}} \cdot \exp \left[\frac{LH_{v0} - \Delta c_p \cdot T_{triple}}{R_v} \cdot \left(\frac{1}{T_{triple}} - \frac{1}{T} \right) \right], \tag{13}$$

where P_{triple} is the vapor pressure at the triple point in Pa, T is the temperature in K, T_{triple} is the temperature at triple point in K, Δc_p is the difference in isobaric specific heat of vapor and liquid in J Kg^{-1} K^{-1}, R_v is the gas constant of water vapor in J Kg^{-1} K^{-1}, and LH_{v0} is the latent heat of vaporization at triple point. Atmospheric vapor pressure was computed using $P_{sat} \cdot$ RH. For each tested environmental cue, we changed only the tested cue while holding all other environmental conditions

225   constant. We ran the sensitivity test in two scenarios: (a) V_{cmax} was uniform throughout the canopy, and (b) V_{cmax} decreased exponentially in lower canopy. For the two scenarios, we let entire canopy mean V_{cmax} be the same (namely mean V_{cmax} at "1X"). We compared the modeled site level NEE, ET, and SIF_{740} among canopy complexity levels.

2.5   Diurnal cycles

To evaluate how much the canopy complexity models differ in real world simulations, we ran the model using weather data from
230   a flux tower located at Ozark, Missouri, USA (US-MOz; Gu et al., 2016). We used the weather and soil moisture data from day 177 to 179 of year 2019 and prescribed leaf temperature and soil water potential to maximally reduce uncertainty among model setups. Briefly, we used outgoing long wave radiation from flux tower measurements to invert canopy temperature and used it as leaf temperature; we also used soil water content to estimate soil water potential and used it as boundary condition for the soil-plant-air continuum. Prescribing leaf temperature and soil water potential allowed us to tease apart the difference caused
235   by canopy complexity from that caused by environmental and physiological differences. See Wang et al. (2021b) for the model setup details for US-MOz. In addition to the observations that were used to set up CliMA Land model (Wang et al., 2021b), we

further applied a vertical V_{cmax} profiles in the simulations (note that V_{cmax} changed in the sunlit and shaded fractions with time for "2X", and stayed constant for the other four complexity levels). We tuned V_{cmax} and whole plant hydraulic conductance to let the "IJKX" predict reasonable NEE and ET, and used these tuned parameters in all the tested canopy complexity levels. We note here that we were not trying to argue one complexity was better than others, but to examine how much the complexity levels differ when we used exactly the same model input parameters.

We compared the model predicted carbon, water, and SIF fluxes. Note it here that observed SIF depends on the sun-sensor geometry, and that SIF retrievals often have different sun-sensor geometry (e.g., the TROPOMI satellite; Köhler et al., 2018). Thus, it is necessary to examine how the sun-sensor geometry may impact the SIF flux across canopy complexity levels. We ran the test using the weather data from (a) 12:00–12:30 pm (b) 16:00–16:30 pm of day 177 in year 2019. At each tested time window, we computed the theoretical SIF at 740 nm for a series of viewing zenith angle from 0° to 85° and relative azimuth angle (angle between sensor and sun) from 0° to 360°. We compared how much the "2KX", "KX", "2X" and "1X" differed from the "IJKX".

Given that averaging APAR theoretically results in overestimated carbon and water fluxes, we expected that the difference among different canopy complexity levels meets the following trends: (a) "1X" > "2X" > "2KX", and (b) "1X" > "KX" > "2KX". Further, as V_{cmax} also theoretically results in overestimated carbon and water fluxes, we expected that adding a vertical V_{cmax} profile further increases the difference in fluxes across canopy complexity levels.

3 Results

3.1 Sensitivity analysis

When a uniform V_{cmax} profile was applied, all tested five canopy complexity levels exhibited similar carbon and water flux responses to changing environmental cues (Figure 4). The responses included increasing canopy photosynthesis and transpiration with higher radiation (Figure 4a), increasing and then decreasing photosynthesis and increasing transpiration with higher temperature (Figure 4b), decreasing photosynthesis and increasing transpiration with higher VPD (Figure 4c), decreasing photosynthesis and transpiration with drier soil (Figure 4d), and increasing photosynthesis and decreasing transpiration with higher atmospheric CO_2 partial pressure (Figure 4e). Further, as expected, "1X", "2X", "KX", "2KX" all overestimated canopy photosynthesis and transpiration compared to "IJKX"mode; and the overestimation ratios met "1X" > "2X" > "2KX" and "1X" > "KX" > "2KX".

The SIF responses to changing environmental cues in general agreed in trends among tested complexity levels (Figure 4). However, SIF responses to radiation, temperature, and atmospheric CO_2 differed dramatically among the five canopy complexity levels given the different response magnitudes (Figure 4b,e). "1X" and "KX" often resulted in different trends compared to "IJKX" (Figure 4). "2X" and "2KX" overall well tracked the SIF responses though slightly overestimated SIF of "IJKX". Notably, we found high disagreement between "2X" and "IJKX" at intermediate radiation, and increasing disagreement at higher atmospheric CO_2 (Figure 4a,e).
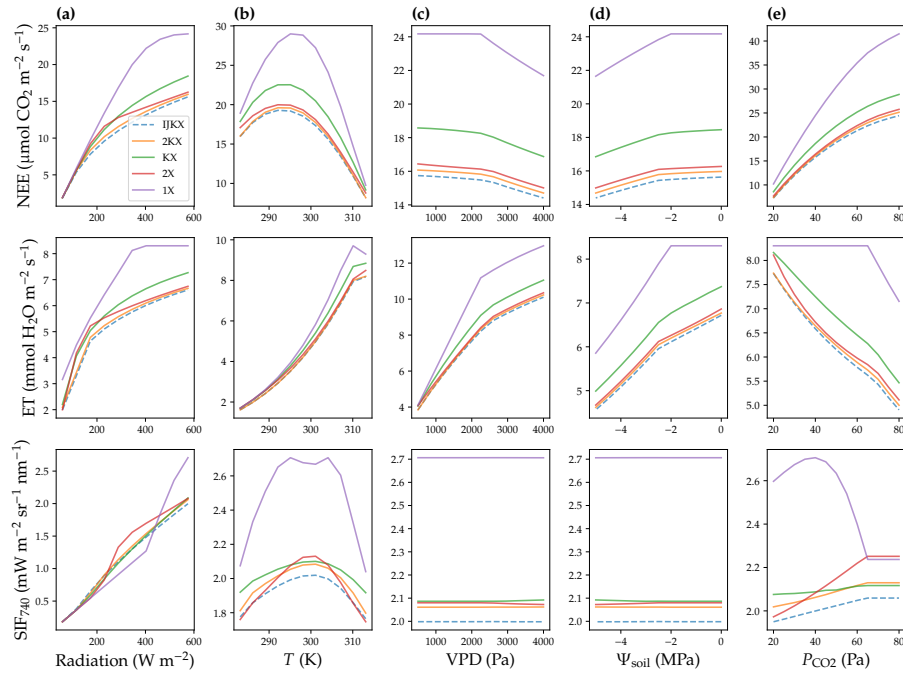
Figure 4. Net ecosystem exchange of CO_2 (NEE, normalized per ground area), evapotranspiration rate (ET, normalized per ground area) and solar induced fluorescence (SIF) responses to changes in environmental cues. **(a)** Responses to total radiation. **(b)** Responses to air and leaf temperature (T). **(c)** Responses to atmospheric vapor pressure deficit (VPD). **(d)** Responses to soil water potential (Ψ_{soil}). **(e)** Responses to atmospheric CO_2 partial pressure (P_{CO2}). This sensitivity analysis was done assuming uniform photosynthetic capacity in the canopy.

When an exponential vertical V_{cmax} profile (lower V_{cmax} in the lower canopy) was applied when simulating canopy fluxes, we found similar trends compared to the scenario with constant V_{cmax} (Figure 5). The differences, however, were that all carbon, water, and SIF fluxes were lower when we applied a vertical V_{cmax} profile (Figure 5). Again, like the scenario of a uniform V_{cmax}, we also found divergent SIF responses to radiation and increasing disagreements among "2X", "2KX" and "IJKX" for elevated CO_2 (Figure 5a,e). The divergent flux responses to P_{CO2} underlined the importance of adopting a more complex canopy ~~concerning the dynamically changing radiation in~~ in future land modeling given that (i) CO_2 concentration within the canopy airspace may change dramatically within a diurnal cycle ~~and rapidly increasing P_{CO2}~~ due to plant carbon fixation, and (ii) atmospheric mean CO_2 is increasing rapidly due to anthropogenic emissions.
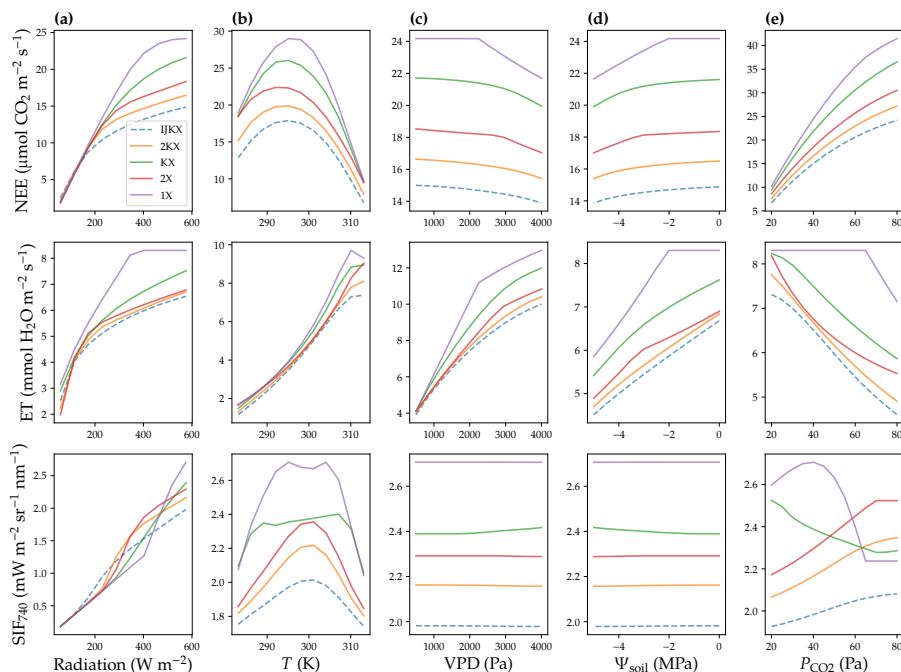
Figure 5. Net ecosystem exchange of CO_2 (NEE, normalized per ground area), evapotranspiration rate (ET, normalized per ground area) and solar induced fluorescence (SIF) responses to changes in environmental cues. **(a)** Responses to total radiation. **(b)** Responses to air and leaf temperature (T). **(c)** Responses to atmospheric vapor pressure deficit (VPD). **(d)** Responses to soil water potential (Ψ_{soil}). **(e)** Responses to atmospheric CO_2 partial pressure (P_{CO2}). This sensitivity analysis was done assuming exponentially decreasing photosynthetic capacity in the lower canopy.

"2KX" and "2X" had lower difference from "IJKX" compared to "KX" and "1X"; and "2KX" had the lowest error given the better resolved APAR fractions (Figures 4–5). Combining all response curves together from Figure 4, we found that when V_{cmax} was evenly distributed in the canopy, relative differences between "2KX" and "IJKX" for carbon, water, and SIF fluxes were 2.4%, 1.2%, and 2.8%, respectively (Figure 6). In comparison, the difference between "2X" and "IJKX" were all higher at 5.4%, 3.8%, and 4.2%, respectively (Figure 6). Overall, the "2KX" had a relative error lower than 5% (Figure 6).
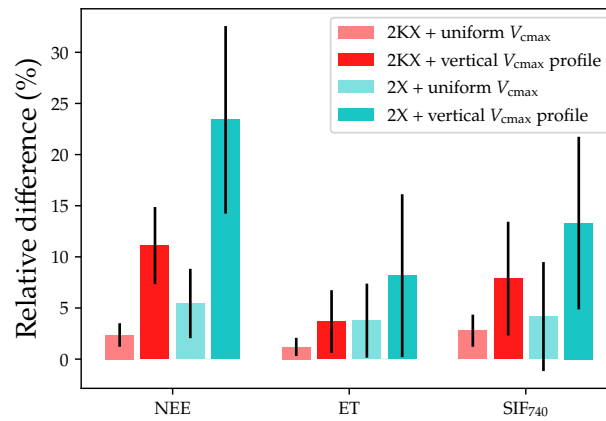
Figure 6. Relative differences among "IJKX", "2KX", and "2X" for net ecosystem exchange of CO_2 (NEE), evapotranspiration (ET), and solar-induced chlorophyll fluorescence (SIF_{740}) fluxes. The lighter bars indicate the case with uniform leaf photosynthetic capacity in the canopy. The darker bars indicate the case with vertical photosynthetic capacity profile (exponentially decreasing capacity in lower canopy). The bars plot relative differences of the fluxes compared to "IJKX" (positive value means overestimated flux).

When accounting for a vertically heterogeneous V_{cmax} profile, we still found lower difference between "2KX" and "IJKX", and the relative differences were 11.1%, 3.7%, and 7.9% (the differences for "2X" were 23.4%, 8.2%, and 13.2%; Figure 6). Overall, the "2KX" had a relative error lower than 10%. Further, the higher error when adopting a vertical V_{cmax} profile agreed
285 with our expectation as the impacts from APAR and V_{cmax} added up (canopy fluorescence was lower for the simpler canopy model at low radiations; Figure 6).

3.2 Diurnal cycle

Our model simulations suggest that all tested canopy complexity levels can qualitatively capture the trends of carbon and water fluxes at the tested flux tower site (Figure 7). However, the tested complexity levels differed dramatically in the magnitudes
290 of carbon and water fluxes. In general, the "1X" had the highest fluxes for both carbon and water fluxes (represented by NEE and ET), followed by "KX", "2X", "2KX", and "IJKX" (Figures 7 and 8). Though "2KX" and "2X", in general, had relatively small differences from "IJKX", we were still able to distinguish the difference (Figures 7 and 8). We note here again that Figures 7 and 8 were meant to highlight the difference between canopy complexity levels in model simulations, but not to say that some models were better than others.
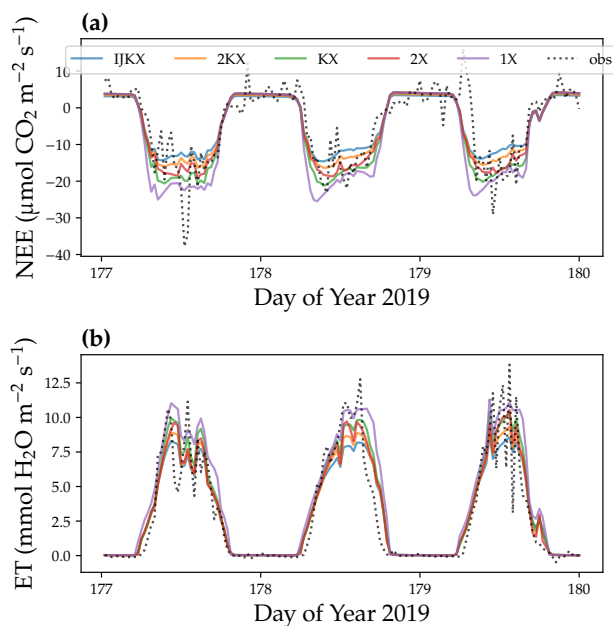
Figure 7. Diurnal cycle of carbon and water fluxes using five different canopy complexity levels. **(a)** Site-level net ecosystem exchange of CO_2 (NEE). **(b)** Site-level evaporation transpiration using plant transpiration as a proxy (ET). The dotted lines were observations from a flux tower at Ozark, Missouri, USA (US-MOz). The colored lines were model simulations with a vertical leaf photosynthetic capacity profile using observed weather drivers from day 177 to 179 of year 2019, such as air and soil humidity. For NEE, more negative value means higher carbon flux; for ET, higher value means higher water flux.
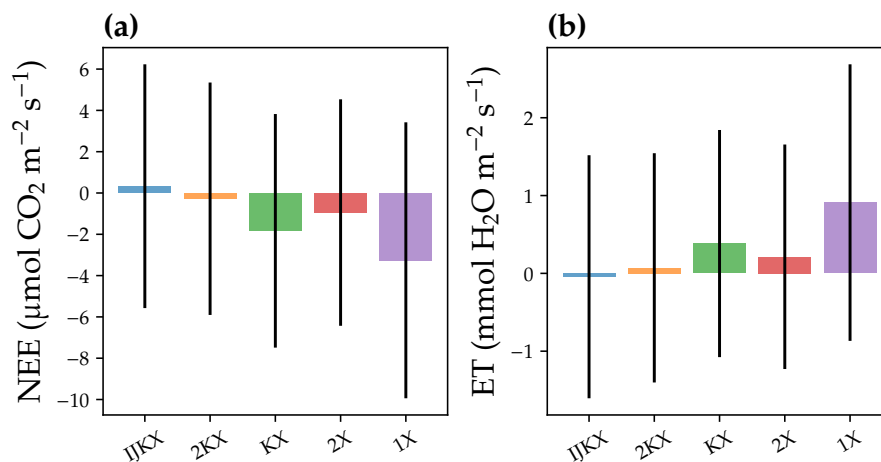
Figure 8. Difference among five different canopy complexity levels in a diurnal cycle simulation of carbon and water fluxes. The carbon flux was represented by site-level net ecosystem exchange of CO_2 (NEE). The water flux was represented by site-level evaporation transpiration using plant transpiration as a proxy (ET). The bars plot the mean difference between model simulation and observations, and error bars plot 1 standard deviation. The observation was from a flux tower at Ozark, Missouri, USA (US-MOz). The model simulations were ran with a vertical leaf photosynthetic capacity profile using observed weather drivers from day 177 to 179 of year 2019, such as air and soil humidity. For NEE, negative values stand for overestimated carbon fluxes; for ET, positive values stand for overestimated water fluxes.

3.3 Sun-sensor geometry

Using less complicated canopy complexity (namely "2KX", "KX", "2X" and "1X") impacted the observed SIF depending on the sun-sensor geometry (Figures 9 and 10). For the tested time window at 12:00–12:30 pm, "2KX" has the least difference from "IJKX", followed by "2X", "KX", and "1X". In general, "2KX" had a difference lower than 11% at any viewing zenith angle or relative azimuth angle for the tested time window (Figures 9). The impact of sun-sensor geometry changed with time because of changes in solar zenith angle and total radiation (e.g., at 16:00–16:30 pm in the afternoon; Figure 10). While "2KX" still had lower overestimated SIF compared to "2X", "KX" had better agreement with "IJKX" and "1X" even underestimated SIF. The dramatic changes in SIF from "KX" and "1X" were due to lower incident radiation from 16:00 to 16:30 pm (Figure 5a).
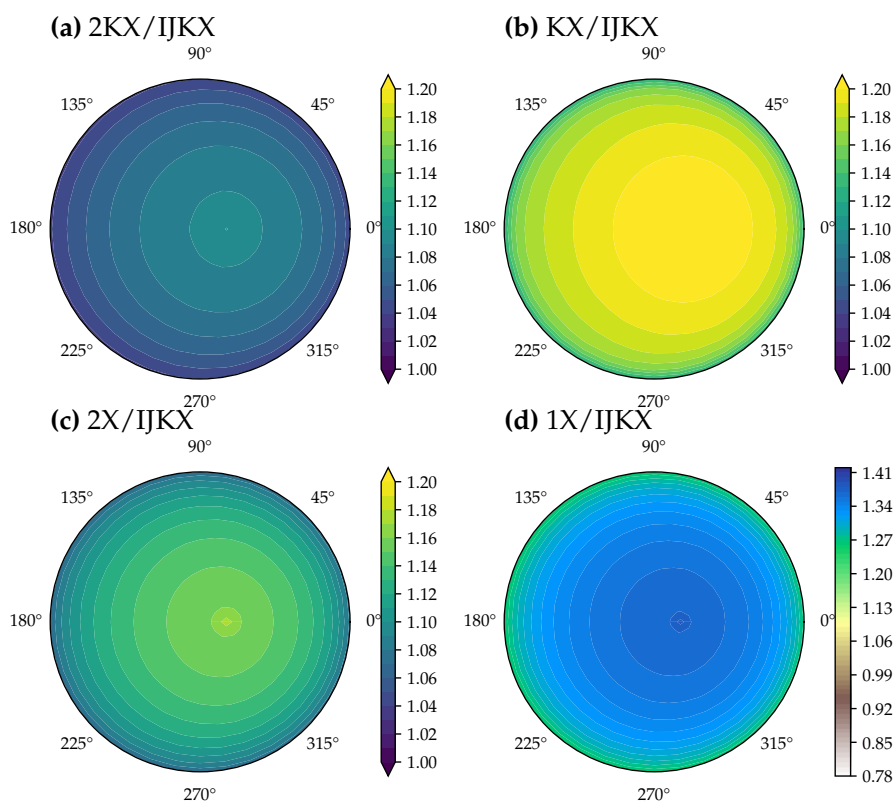
Figure 9. Difference among five different canopy complexity levels in modeled solar-induced chlorophyll fluorescence (SIF) at different viewing zenith angle and relative azimuth angle. The color indicates the SIF at 740 nm of tested canopy complexity level relative to "IJKX". The model simulations were ran with a vertical leaf photosynthetic capacity profile using observed weather drivers during 12:00–12:30 pm of day 177 in year 2019 at a flux tower at Ozark, Missouri, USA (US-MOz).
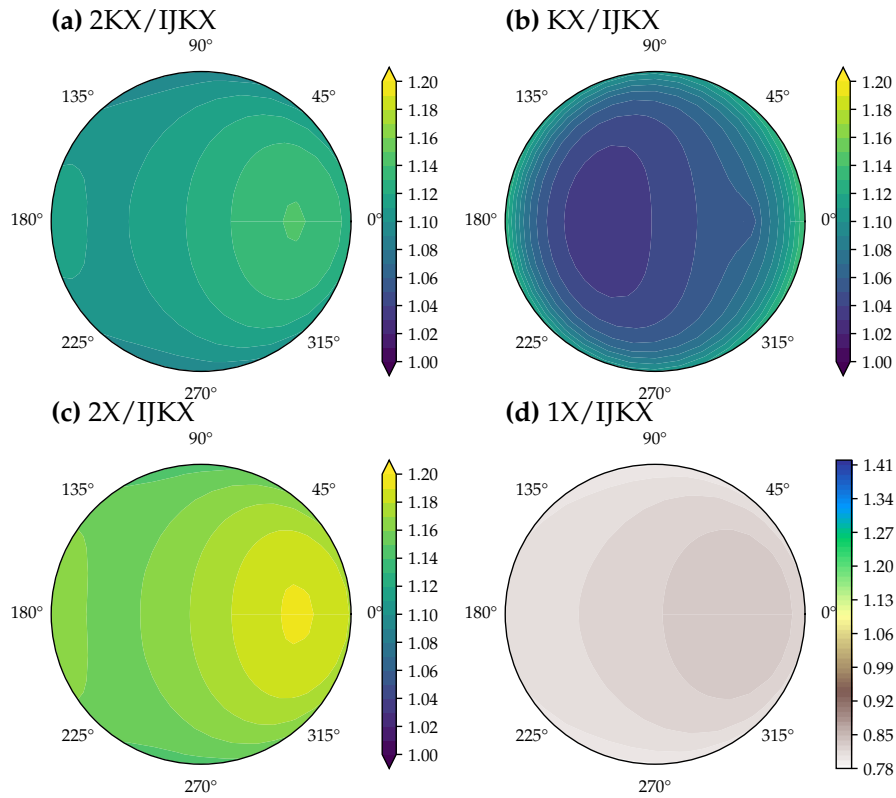
Figure 10. Difference among five different canopy complexity levels in modeled solar-induced chlorophyll fluorescence (SIF) at different viewing zenith angle and relative azimuth angle. The color indicates the SIF at 740 nm of tested canopy complexity relative to "IJKX". The model simulations were ran with a vertical leaf photosynthetic capacity profile using observed weather drivers during 16:00–16:30 pm of day 177 in year 2019 at a flux tower at Ozark, Missouri, USA (US-MOz).

4 Discussion

4.1 Fluorescence and radiation

While simpler canopy models in general predicted higher carbon, water, and SIF fluxes, there were some scenarios that the simpler models predict contrasting SIF responses compared to "IJKX": (a) when total radiation increased, SIF of the simpler canopy models were lower than "IJKX" at low radiation, but were higher than "IJKX" at high radiation (Figures 4 and 5); (b) "1X" model SIF increased and then decreased and stayed unchanged with higher atmospheric CO_2 (Figures 4 and 5); and (c) "KX" model SIF increased marginally with higher atmospheric CO_2 for a canopy without vertical V_{cmax} gradient, but decreased with higher CO_2 for a canopy with vertical V_{cmax} profile (Figures 4 and 5). These contrasting patterns of the simpler models resulted from the different photosynthesis system II (PSII) quantum yield and fluorescence quantum yield (~~FQE~~namely ϕ_F) responses to APAR and CO_2 (Figure 11a,b). PSII quantum yield measures efficiency of converting absorbed photons to electrons by PSII; and ϕ_F measures the efficiency of converting absorbed photons to fluorescence photons. The PSII yield increases and then saturates with higher leaf internal CO_2 and lower APAR. In our model, ~~the FQE~~ ϕ_F follows the parameterization of van der Tol et al. (2014) but fitted on leaves measured by Flexas et al. (2002), as first used in Lee et al. (2015). Typically, ~~the PSII to FQE~~ PSII to ϕ_F relationship depends on the state of non-photochemical quenching (NPQ; Porcar-Castell et al., 2014). ~~FQE~~The ϕ_F has a maximum at intermediate PSII levels (around 0.6) but ~~decrease~~ decreases at lower PSII yields (increased NPQ) as well as higher PSII yields (increased competition with photochemical quenching). This general behavior explains what we see: ~~FQE~~ ϕ_F (a) stays unchanged at low radiation with higher leaf internal CO_2, (b) increases and then decreases and stays unchanged with higher leaf internal CO_2 at intermediate APAR, (c) increased with higher CO_2 at high CO_2, and (d) increases and then decreases with higher APAR (Figure 11a,b). Though ~~FQE~~ ϕ_F in general agrees with the PSII yield patterns at high APAR (typical experimental and top-of-canopy scenarios), the disagreements at low APAR could result in problems when APAR is inappropriately averaged. In our case, the turnover from APAR regions in which PSII and ~~FQE~~ ϕ_F are anticorrelated (light-limited) to the region in which they are correlated (increase in NPQ) happens at around 200 μmol m^2 s^{-1}.

When total radiation was higher, the product of ~~FQE~~ ϕ_F and APAR (leaf level SIF) increased (Figure 11c). When ~~FQE~~ ϕ_F stayed unchanged at low APAR, leaf level SIF increases linearly with higher APAR, and SIF increases faster when ~~FQE~~ ϕ_F starts to increase after a certain threshold (the threshold increased with higher leaf internal CO_2; Figure 11b). Then leaf level SIF slowed down with higher APAR due to decreasing ~~FQE~~ ϕ_F at higher APAR, and was higher when leaf internal CO_2 was higher (Figure 11b,c). As leaf internal CO_2 was theoretically lowest for "1X", and then followed by "KX", "2X", and "2KX" given the way APAR was averaged, it was expected that "2KX" increased earliest with higher APAR and that "1X" had highest SIF at high radiation (Figures 4a and 5a). Therefore, in the diurnal cycle simulations, "1X" SIF overestimated SIF at noon when radiation was high (Figure 9), but underestimated SIF in the late afternoon as a result of lower radiation (Figure 10). The inconsistent SIF patterns at low and high radiation from simpler canopy models may potentially result in biases in modeled diurnal and seasonal SIF, and thus we suggest to use a complex canopy model when possible to minimize the impact from heterogeneous canopy radiation and leaf physiology.
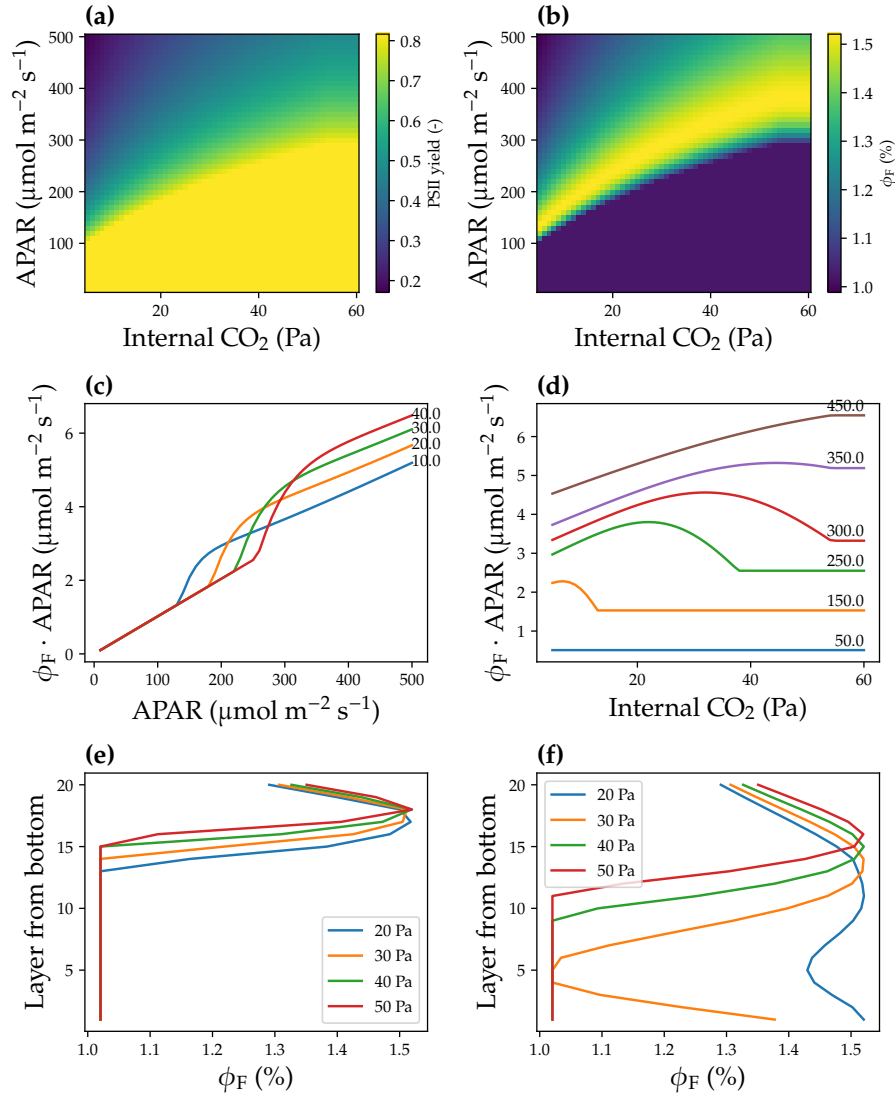
Figure 11. Leaf fluorescence responses to radiation, CO_2 partial pressure, and leaf maximum carboxylation rate. **(a)** Photosynthesis system II quantum yield responses to leaf absorbed photosynthetically active radiation (APAR) and leaf internal CO_2 partial pressure. **(b)** Leaf fluorescence quantum yield (~~FQE~~ ϕ_F) responses to APAR and leaf internal CO_2. **(c)** Product of ~~FQE~~ ϕ_F and APAR vs. APAR for leaves with different internal CO_2 (number labeled next to each curve; unit: Pa). **(d)** Product of ~~FQE~~ ϕ_F and APAR vs. internal CO_2 at different APAR (number labeled next to each curve; unit μmol m^{-2} s^{-1}). The simulations of panels a–d are done at a leaf temperature of 25 °C and a maximum carboxylation rate (V_{cmax}) of 60 μmol CO_2 m^{-2} s^{-1}. **(e)** ~~FQE~~ The ϕ_F of different canopy layers at a given atmospheric CO_2 partial pressure. V_{cmax} was the same among canopy layers. The simulation results are from Figure 4e. **(f)** ~~FQE~~ The ϕ_F of different canopy layers at a given atmospheric CO_2. V_{cmax} was lower in the lower canopy. The simulation results are from Figure 5e.

"1X" model SIF response to atmospheric CO_2 ought to depend on the mean canopy APAR (Figure 11b): (a) if mean APAR was low, "1X" SIF should stay constant with higher CO_2, (b) if mean APAR was moderate, "1X" SIF ought to increase, and then decrease and stay constant with higher CO_2, and (c) if mean APAR was high, "1X" SIF would increase with higher CO_2 (Figure 11b,d). For the simulations in Figures 4 and 5, mean APAR was 156 μmol m^{-2} s^{-1}, and thus "1X" SIF increased and then decreased with higher CO_2.

"KX" model SIF response to atmospheric CO_2 was impacted by both leaf internal CO_2 and vertical APAR profile given the heterogeneous APAR. As ~~FQE~~ ϕ_F was higher in the middle layers at lower atmospheric CO_2 when there is no vertical V_{cmax} gradient, modeled SIF showed marginal increase with higher CO_2 (Figures 4 and 11e). However, when there was a vertical V_{cmax} gradient, ~~FQE~~ ϕ_F was much higher in the lower canopy at lower CO_2, potentially resulting a higher SIF at low atmospheric CO_2 which was contrary to "IJKX" prediction. The erroneous predicted SIF patterns of "1X" and "KX" highlighted the importance of appropriately averaged leaf APAR, particularly the partitioning of sunlit and shaded leaves.

4.2 Dataset compatibility

Our model simulations showed that different canopy complexity levels predicted divergent carbon, water, and SIF fluxes. The "1X" and "KX" without partitioning the canopy to sunlit and shaded fractions, in particular, showed very high biases compared to the other three levels of complexity, namely "2X", "2KX", and "IJKX". Further, as we expected, "IJKX" that has the most complex canopy had the lowest predicted carbon and water fluxes, followed by "2KX" and "2X" and then "KX" and "1X". Moreover, when we accounted for vertical canopy photosynthetic capacity profile, the difference among canopy complexity levels increased. Though "2KX" and "2X" were, in general, close to "IJKX" in predicted canopy fluxes, the disagreements may range up to > 20% (maximum) for "2KX" and up to > 40% (maximum) for "2X". Given the differences in predicted fluxes using different canopy complexity levels, and the varying difference (not a constant ratio), we do not recommend using photosynthetic parameters inverted from different canopy complexity models, i.e. parameter fitting has to be performed with the same underlying model as for the full forward modeling. Given the higher realism of the enhanced complexity models, however, leaf level fits of photosynthetic parameters could be employed in models of higher complexity but would result in high biases when used in simple ~~big-leaf~~ big leaf models.

The disagreements among canopy complexity levels make it difficult to parameterize a land model using complex canopy setup, and thus hamper the fusion of large scale remote sensing based datasets with land models at global scale. Thus, it is necessary to revisit the flux and plant trait inversions using more applicable land model setups to make sure the inverted datasets and land models are consistent in their assumptions. This is the only way to ensure that inverted parameters are quantitatively useful in future land surface modeling. Moreover, it is also possible for land models to go without the inverted fluxes or traits if the land model runs using a complex canopy such as "IJKX". This way, the model can be directly compared against satellite observations (Shiklomanov et al., 2021) without an intermediate step that performs the inversion from radiation observations canopy properties and thus surface water and carbon fluxes.

4.3 Necessity of a complex canopy

As suggested by Bonan et al. (2021), modelers need to move to a multi-layered canopy modeling to account for the vertical profiles and microclimates in the canopy. Further, to better utilize the broadly available remote sensing data, modelers need to move from broadband radiation to hyperspectral radiation and from sun/shade fractions to leaf angular distribution. One may ask whether it is necessary to implement a way more complex and inefficient multi-layered canopy with leaf angular distributions to account for an average 5%–22% difference, while the difference can be compensated by tuning plant traits such as photosynthetic capacity and hydraulic conductance. The answer varies depending on what types of data are used in the model. If one uses parameters meant to use with "2X" (namely a ~~big-leaf~~ two-leaf canopy), using a multi-layered canopy such as "2KX" and "IJKX" would not improve the model performance, but instead could result in higher biases. In this case, we suggest to keep the same canopy complexity as used to derive plant traits. However, if one wants to bridge plant physiology to both leaf-level measurements as well as remotely sensed data such as the reflection and fluorescence spectra, we would suggest using "IJKX" or using even more complicated canopy model to be as accurate as possible. We note here that "2KX" approximates the "IJKX" well with an average 3%-12% difference, and "2KX" would be useful to speed the calculations for more qualitatively oriented research as the trends generally agree between "2KX" and "IJKX".

We recognize that increasing model complexity can make it (a) less user-friendly for researchers to use (e.g., when implementing the model into their research projects), and (b) slower to run the model, particularly using less efficient programming languages such as Python and R (compared to C). In our highly modularized CliMA Land model, we use Julia, a just-in-time compiled programming language that allows the versatility of a scripting language like python but with the speed of fully compiled languages such as C and Fortran; https://julialang.org/benchmarks/). The CliMA Land model can simulate canopy radiation using either the mSCOPE-based radiative transfer scheme (Yang et al., 2017) or the traditional sunlit and shaded fraction scheme (e.g., De Pury and Farquhar, 1997; Campbell and Norman, 1998). Further, CliMA Land supports both stomatal optimization models (including those from Sperry et al., 2017; Anderegg et al., 2018; Eller et al., 2018; Wang et al., 2020) and empirical stomatal models (including those from Ball et al., 1987; Leuning, 1995; Medlyn et al., 2011). For the empirical stomatal models, CliMA Land supports using an ad-hoc tuning factor to account for stomatal responses to soil moisture through tuning either the empirical fitting parameter (such as g_1 in Ball et al. (1987) and Medlyn et al. (2011) models) or leaf photosynthetic capacity ~~(as did in Kennedy et al., 2019)~~ (as done in Kennedy et al., 2019). Users may freely customize the model setup by choosing among provided alternatives. We believe the practice of making land models more open and modular will benefit the land model and plant physiology communities in future research.

5 Conclusions

We evaluated how much canopy carbon, water, and SIF fluxes differ when using five different canopy complexity levels in a land model. We found that when using the same model inputs, simpler canopy models predicted higher carbon, water, and SIF fluxes; and when we accounted for a vertically heterogeneous photosynthetic capacity profile, we found more disagreements among canopy models with varying complexity levels. We also found that the modeled SIF varied with sun-sensor geometry

among tested canopy complexity levels. Our model results suggest that misusing parameters inverted from different canopy complexities and assumptions may resulted in biases in predicted canopy fluxes, and thus we recommend more cautious model parameterization regarding canopy complexity levels. Further, we recommend using complex canopy models with leaf angular distribution and hyperspectral canopy radiative transfer scheme to compare against remote sensing data in order to accurately mimic observed radiation. However, the use of complex canopy models in land surface modeling may be less efficient and not user-friendly to researchers. We believe more open and modular land models like CliMA Land will help lower the threshold to researchers.

Code and data availability. We coded our model and did the analysis using Julia (version 1.6.2), and current version of the CliMA Land model is available from the project website: https://github.com/CliMA/Land under the Apache 2.0 License.

Author contributions. YW and CF designed and conducted the research, performed the general data analysis, and wrote the paper.

Competing interests. No competing interests

Acknowledgements. ~~This research was made possible by Hopewell Fund and by the generosity~~ We gratefully acknowledge the generous support of Eric and Wendy Schmidt (by recommendation of the Schmidt Futures ~~program~~) and the Heising-Simons Foundation. CF was supported by NASA OCO 2/3 science team grant no. 80NSSC18K0895.

References

Anderegg, W. R., Wolf, A., Arango-Velez, A., Choat, B., Chmura, D. J., Jansen, S., Kolb, T., Li, S., Meinzer, F. C., Pita, P., et al.: Woody plants optimise stomatal behaviour relative to hydraulic risk, Ecology Letters, 21, 968–977, 2018.

420 Badgley, G., Anderegg, L. D., Berry, J. A., and Field, C. B.: Terrestrial gross primary production: Using NIRV to scale from site to globe, Global change biology, 25, 3731–3740, 2019.

Ball, J. T., Woodrow, I. E., and Berry, J. A.: A model predicting stomatal conductance and its contribution to the control of photosynthesis under different environmental conditions, in: Progress in photosynthesis research, pp. 221–224, Springer, 1987.

Bonan, G. B., Lawrence, P. J., Oleson, K. W., Levis, S., Jung, M., Reichstein, M., Lawrence, D. M., and Swenson, S. C.: Improving canopy
425 processes in the Community Land Model version 4 (CLM4) using global flux fields empirically inferred from FLUXNET data, Journal of Geophysical Research: Biogeosciences, 116, 2011.

Bonan, G. B., Patton, E. G., Harman, I. N., Oleson, K. W., Finnigan, J. J., Lu, Y., and Burakowski, E. A.: Modeling canopy-induced turbulence in the Earth system: A unified parameterization of turbulent exchange within plant canopies and the roughness sublayer (CLM-ml v0), Geoscientific Model Development, 11, 1467–1496, 2018.

430 Bonan, G. B., Patton, E. G., Finnigan, J. J., Baldocchi, D. D., and Harman, I. N.: Moving beyond the incorrect but useful paradigm: reeval-uating big-leaf and multilayer plant canopies to model biosphere-atmosphere fluxes–a review, Agricultural and Forest Meteorology, 306, 108 435, 2021.

Boone, A., Samuelsson, P., Gollvik, S., Napoly, A., Jarlan, L., Brun, E., and Decharme, B.: The interactions between soil–biosphere–atmosphere land surface model with a multi-energy balance (ISBA-MEB) option in SURFEXv8–Part 1: Model description, Geoscientific
435 Model Development, 10, 843–872, 2017.

Braghiere, R. K., Wang, Y., Doughty, R., Sousa, D., Magney, T., Widlowski, J.-L., Longo, M., Bloom, A. A., Worden, J., Gentine, P., et al.: Accounting for canopy structure improves hyperspectral radiative transfer and sun-induced chlorophyll fluorescence representations in a new generation Earth System model, Remote Sensing of Environment, 261, 112 497, 2021.

Campbell, G. S. and Norman, J. M.: An introduction to environmental biophysics, Springer Science & Business Media, New York, New
440 York, USA, 1998.

Carrer, D., Roujean, J.-L., Lafont, S., Calvet, J.-C., Boone, A., Decharme, B., Delire, C., and Gastellu-Etchegorry, J.-P.: A canopy radiative transfer scheme with explicit FAPAR for the interactive vegetation model ISBA-A-gs: Impact on carbon fluxes, Journal of Geophysical Research: Biogeosciences, 118, 888–903, 2013.

Chen, J., Liu, J., Cihlar, J., and Goulden, M.: Daily canopy photosynthesis model through temporal and spatial scaling for remote sensing
445 applications, Ecological modelling, 124, 99–119, 1999.

Chen, J. M., Mo, G., Pisek, J., Liu, J., Deng, F., Ishizawa, M., and Chan, D.: Effects of foliage clumping on the estimation of global terrestrial gross primary productivity, Global Biogeochemical Cycles, 26, 2012.

Chen, Y., Ryder, J., Bastrikov, V., McGrath, M. J., Naudts, K., Otto, J., Ottlé, C., Peylin, P., Polcher, J., Valade, A., et al.: Evaluating the performance of land surface model ORCHIDEE-CAN v1. 0 on water and energy flux estimation with a single-and multi-layer energy
450 budget scheme, Geoscientific Model Development, 9, 2951–2972, 2016.

Clark, D., Mercado, L., Sitch, S., Jones, C., Gedney, N., Best, M., Pryor, M., Rooney, G., Essery, R., Blyth, E., et al.: The Joint UK Land Environment Simulator (JULES), model description–Part 2: carbon fluxes and vegetation dynamics, Geoscientific Model Development, 4, 701–722, 2011.

Colombo, R., Bellingeri, D., Fasolini, D., and Marino, C. M.: Retrieval of leaf area index in different vegetation types using high resolution satellite data, Remote Sensing of Environment, 86, 120–131, 2003.

Croft, H., Chen, J., Wang, R., Mo, G., Luo, S., Luo, X., He, L., Gonsamo, A., Arabian, J., Zhang, Y., et al.: The global distribution of leaf chlorophyll content, Remote Sensing of Environment, 236, 111 479, 2020.

De Pury, D. and Farquhar, G.: Simple scaling of photosynthesis from leaves to canopies without the errors of big-leaf models, Plant, Cell & Environment, 20, 537–557, 1997.

Deng, F., Chen, J. M., Plummer, S., Chen, M., and Pisek, J.: Algorithm for global leaf area index retrieval using satellite imagery, IEEE transactions on geoscience and remote sensing, 44, 2219–2229, 2006.

Eller, C. B., Rowland, L., Oliveira, R. S., Bittencourt, P. R. L., Barros, F. V., da Costa, A. C. L., Meir, P., Friend, A. D., Mencuccini, M., Sitch, S., and Cox, P.: Modelling tropical forest responses to drought and El Niño with a stomatal optimization model based on xylem hydraulics, Philosophical Transactions of the Royal Society B: Biological Sciences, 373, 20170 315, 2018.

Farquhar, G. D., von Caemmerer, S., and Berry, J. A.: A biochemical model of photosynthetic CO_2 assimilation in leaves of C_3 species, Planta, 149, 78–90, 1980.

Flexas, J., Escalona, J. M., Evain, S., Gulías, J., Moya, I., Osmond, C. B., and Medrano, H.: Steady-state chlorophyll fluorescence (Fs) measurements as a tool to follow variations of net CO2 assimilation and stomatal conductance during water-stress in C3 plants, Physiologia plantarum, 114, 231–240, 2002.

Frankenberg, C., Fisher, J. B., Worden, J., Badgley, G., Saatchi, S. S., Lee, J.-E., Toon, G. C., Butz, A., Jung, M., Kuze, A., et al.: New global observations of the terrestrial carbon cycle from GOSAT: Patterns of plant fluorescence with gross primary productivity, Geophysical Research Letters, 38, 2011.

Gu, L., Pallardy, S. G., Yang, B., Hosman, K. P., Mao, J., Ricciuto, D., Shi, X., and Sun, Y.: Testing a land model in ecosystem functional space via a comparison of observed and modeled ecosystem flux responses to precipitation regimes and associated stresses in a Central US forest, Journal of Geophysical Research: Biogeosciences, 121, 1884–1902, 2016.

Jogireddy, V. R., Cox, P. M., Huntingford, C., Harding, R. J., and Mercado, L.: An improved description of canopy light interception for use in a GCM land-surface scheme: calibration and testing against carbon fluxes at a coniferous forest, Met Office Exeter, UK, 2006.

Kennedy, D., Swenson, S., Oleson, K. W., Lawrence, D. M., Fisher, R., Lola da Costa, A. C., and Gentine, P.: Implementing plant hydraulics in the community land model, version 5, Journal of Advances in Modeling Earth Systems, 11, 485–513, 2019.

Köhler, P., Frankenberg, C., Magney, T. S., Guanter, L., Joiner, J., and Landgraf, J.: Global retrievals of solar-induced chlorophyll fluorescence with TROPOMI: First results and intersensor comparison to OCO-2, Geophysical Research Letters, 45, 10,456–10,463, 2018.

Lawrence, D. M., Fisher, R. A., Koven, C. D., Oleson, K. W., Swenson, S. C., Bonan, G., Collier, N., Ghimire, B., Van Kampenhout, L., Kennedy, D., et al.: The Community Land Model version 5: Description of new features, benchmarking, and impact of forcing uncertainty, Journal of Advances in Modeling Earth Systems, 11, 4245–4287, 2019.

Lee, J.-E., Berry, J. A., van der Tol, C., Yang, X., Guanter, L., Damm, A., Baker, I., and Frankenberg, C.: Simulations of chlorophyll fluorescence incorporated into the C ommunity L and M odel version 4, Global change biology, 21, 3469–3477, 2015.

Leuning, R.: A critical appraisal of a combined stomatal-photosynthesis model for C_3 plants, Plant, Cell & Environment, 18, 339–355, 1995.

Luo, X., Chen, J. M., Liu, J., Black, T. A., Croft, H., Staebler, R., He, L., Arain, M. A., Chen, B., Mo, G., et al.: Comparison of big-leaf, two-big-leaf, and two-leaf upscaling schemes for evapotranspiration estimation using coupled carbon-water modeling, Journal of Geophysical Research: Biogeosciences, 123, 207–225, 2018.

Medlyn, B. E., Duursma, R. A., Eamus, D., Ellsworth, D. S., Prentice, I. C., Barton, C. V. M., Crous, K. Y., de Angelis, P., Freeman, M., and Wingate, L.: Reconciling the optimal and empirical approaches to modelling stomatal conductance, Global Change Biology, 17, 2134–2144, 2011.

Momen, M., Wood, J. D., Novick, K. A., Pangle, R., Pockman, W. T., McDowell, N. G., and Konings, A. G.: Interacting effects of leaf water potential and biomass on vegetation optical depth, Journal of Geophysical Research: Biogeosciences, 122, 3031–3046, 2017.

Monteith, J. L.: Evaporation and environment, in: Symposia of the society for experimental biology, vol. 19, pp. 205–234, Cambridge University Press (CUP) Cambridge, 1965.

Norman, J., Anderson, M., Kustas, W., French, A., Mecikalski, J., Torn, R., Diak, G., Schmugge, T., and Tanner, B.: Remote sensing of surface energy fluxes at 101-m pixel resolutions, Water Resources Research, 39, 2003.

Norman, J. M.: Simulation of microclimates, Biometeorology in integrated pest management, pp. 65–99, 1982.

Penman, H. L.: Natural evaporation from open water, bare soil and grass, Proceedings of the Royal Society of London. Series A. Mathematical and Physical Sciences, 193, 120–145, 1948.

Porcar-Castell, A., Tyystjärvi, E., Atherton, J., Van der Tol, C., Flexas, J., Pfündel, E. E., Moreno, J., Frankenberg, C., and Berry, J. A.: Linking chlorophyll a fluorescence to photosynthesis for remote sensing applications: mechanisms and challenges, Journal of experimental botany, 65, 4065–4095, 2014.

Roerink, G., Su, Z., and Menenti, M.: S-SEBI: A simple remote sensing algorithm to estimate the surface energy balance, Physics and Chemistry of the Earth, Part B: Hydrology, Oceans and Atmosphere, 25, 147–157, 2000.

Ryder, J., Polcher, J., Peylin, P., Ottlé, C., Chen, Y., van Gorsel, E., Haverd, V., McGrath, M. J., Naudts, K., Otto, J., et al.: A multi-layer land surface energy budget model for implicit coupling with global atmospheric simulations, Geoscientific Model Development, 9, 223–245, 2016.

Sellers, P., Berry, J., Collatz, G., Field, C., and Hall, F.: Canopy reflectance, photosynthesis, and transpiration. III. A reanalysis using improved leaf models and a new canopy integration scheme., Remote sensing of environment, 42, 187–216, 1992.

Shan, N., Zhang, Y., Chen, J. M., Ju, W., Migliavacca, M., Peñuelas, J., Yang, X., Zhang, Z., Nelson, J. A., and Goulas, Y.: A model for estimating transpiration from remotely sensed solar-induced chlorophyll fluorescence, Remote Sensing of Environment, 252, 112 134, 2021.

Shiklomanov, A. N., Dietze, M. C., Fer, I., Viskari, T., and Serbin, S. P.: Cutting out the middleman: calibrating and validating a dynamic vegetation model (ED2-PROSPECT5) using remotely sensed surface reflectance, Geoscientific Model Development, 14, 2603–2633, 2021.

Sperry, J. S., Wang, Y., Wolfe, B. T., Mackay, D. S., Anderegg, W. R. L., McDowell, N. G., and Pockman, W. T.: Pragmatic hydraulic theory predicts stomatal responses to climatic water deficits, New Phytologist, 212, 577–589, 2016.

Sperry, J. S., Venturas, M. D., Anderegg, W. R. L., Mencuccini, M., Mackay, D. S., Wang, Y., and Love, D. M.: Predicting stomatal responses to the environment from the optimization of photosynthetic gain and hydraulic cost, Plant, Cell & Environment, 40, 816–830, 2017.

Sprintsin, M., Chen, J. M., Desai, A., and Gough, C. M.: Evaluation of leaf-to-canopy upscaling methodologies against carbon flux data in North America, Journal of Geophysical Research: Biogeosciences, 117, G01 023, 2012.

Sun, Y., Frankenberg, C., Jung, M., Joiner, J., Guanter, L., Köhler, P., and Magney, T.: Overview of Solar-Induced chlorophyll Fluorescence (SIF) from the Orbiting Carbon Observatory-2: Retrieval, cross-mission comparison, and global monitoring for GPP, Remote Sensing of Environment, 209, 808–823, 2018.

Van der Tol, C., Verhoef, W., Timmermans, J., Verhoef, A., and Su, Z.: An integrated model of soil-canopy spectral radiances, photosynthesis, fluorescence, temperature and energy balance., Biogeosciences, 6, 2009.

530 van der Tol, C., Berry, J., Campbell, P., and Rascher, U.: Models of fluorescence and photosynthesis for interpreting measurements of solar-induced chlorophyll fluorescence, Journal of Geophysical Research: Biogeosciences, 119, 2312–2327, 2014.

Wang, Y., Sperry, J. S., Anderegg, W. R. L., Venturas, M. D., and Trugman, A. T.: A theoretical and empirical assessment of stomatal optimization modeling, New Phytologist, 227, 311–325, 2020.

Wang, Y., Anderegg, W. R., Venturas, M. D., Trugman, A. T., Yu, K., and Frankenberg, C.: Optimization theory explains nighttime stomatal

535 responses, New Phytologist, 230, 1550–1561, https://doi.org/10.1111/nph.17267, 2021a.

Wang, Y., Köhler, P., He, L., Doughty, R., Braghiere, R. K., Wood, J. D., and Frankenberg, C.: Testing stomatal models at stand level in deciduous angiosperm and evergreen gymnosperm forests using CliMA Land (v0.1), Geoscientific Model Development Discussions, 2021, 1–35, https://doi.org/10.5194/gmd-2021-154, 2021b.

Wang, Y.-P. and Leuning, R.: A two-leaf model for canopy conductance, photosynthesis and partitioning of available energy I:: Model

540 description and comparison with a multi-layered model, Agricultural and Forest Meteorology, 91, 89–111, 1998.

Yang, P., Verhoef, W., and van der Tol, C.: The mSCOPE model: A simple adaptation to the SCOPE model to describe reflectance, fluorescence and photosynthesis of vertically heterogeneous canopies, Remote sensing of environment, 201, 1–11, 2017.

Yang, P., Prikaziuk, E., Verhoef, W., and van der Tol, C.: SCOPE 2.0: a model to simulate vegetated land surface fluxes and satellite signals, Geoscientific Model Development, 14, 4697–4712, https://doi.org/10.5194/gmd-14-4697-2021, 2021.

545 Zhang, Y., Guanter, L., Berry, J. A., van der Tol, C., Yang, X., Tang, J., and Zhang, F.: Model-based analysis of the relationship between sun-induced chlorophyll fluorescence and gross primary production for remote sensing applications, Remote Sensing of Environment, 187, 145–155, 2016.

Zhang, Y., Zhou, S., Gentine, P., and Xiao, X.: Can vegetation optical depth reflect changes in leaf water potential during soil moisture dry-down events?, Remote Sensing of Environment, 234, 111 451, 2019.